



Dissimilar mechanism of executing hole transfer by WO₃ and MoO₃ nanoparticles in organic solar cells



Eung-Kyu Park, Jae-Hyoung Kim, Ji-Hwan Kim, Min-Ho Park, Dong-Hoon Lee, Yong-Sang Kim*

School of Electronic and Electrical Engineering, Sungkyunkwan University, Suwon 440-746, Republic of Korea

ARTICLE INFO

Available online 12 December 2014

Keywords:

Organic solar cells
Metal oxides
Tungsten oxide
Molibdenum oxide
Nanoparticles
PEDOT:PSS
P3HT:PCBM

ABSTRACT

We investigated the effect of metal oxide nanoparticles (NPs) in poly (3,4 ethylenedioxythiophene):poly (styrene-sulfonate) layer for the light harvestation in poly (3-hexylthiophene):[6,6]-phenyl-C₆₁-butyric acid methyl ester organic solar cells. The role of tungsten trioxide nanoparticles (WO₃) and molybdenum trioxide nanoparticles (MoO₃) in enhancing the efficiency of solar cells was compared. Due to the difference in the energy band structure of the two nanoparticles, the WO₃ NPs acted as a hole blocking layer, whereas MoO₃ NPs helped in the hole transfer. The solar cell with WO₃ NPs at 1.5 wt% concentration showed a power conversion efficiency of 4.22% under AM 1.5G illumination and the device blended with 2 wt% of MoO₃ NPs showed a power conversion efficiency of 4.40%. We measured various electrical properties including, electrochemical impedance spectroscopy and recombination mechanisms using the light intensity dependent current–voltage measurement of organic solar cell.

© 2014 Elsevier B.V. All rights reserved.

1. Introduction

The organic solar cells (OSCs) have an infinite potential of becoming a renewable energy source because of the advantages like low-cost, simple fabrication, light-weight, and flexibility [1–3]. However, in the polymer and fullerene blend, the charge carrier mobility is comparatively low with a short exciton diffusion length in the active layer, which limits the power conversion efficiency (PCE) of the devices [4]. The short-circuit current density (J_{sc}) and PCE of solar cells depend on the efficient harvesting of light and efficient charge separation.

The scattering of light due to the surface plasmon resonance effect is the most sought-after technique to enhance the J_{sc} of organic solar cells [5]. The addition of light scattering materials revamps the intensity of light in the device, resulting in an increased light absorption. The metallic NPs can be used as an optical spacer in the buffer layer (Au, MoO₃, CsCO₃, V₂O₅, ZnO, Ca) [6–11]. A number of reports focus on the thermal evaporation, chemical vapor deposition, or sputtering of the metallic nanoparticle (NPs). Other hole-injecting polymers with larger work functions have also been synthesized to enhance the hole injection [12,13]. Inorganic layers of transition metal oxides have been discussed as an alternative to poly (3,4 ethylenedioxythiophene):Poly (styrene-sulfonate) (PEDOT:PSS), such as vanadium (III) oxide (V₂O₃) and molybdenum trioxide (MoO₃) vacuum deposited onto the indium tin oxide (ITO) in OSCs [10]. Although these techniques proved to be

effective; commercial or bulk production of these devices will take longer fabrication time and are much expensive.

However, the approach addressed in this paper is the careful use of metallic nanoparticle's properties to induce surface plasmons, which increases the optical absorption and photocurrent generation over a broad range of visible wavelengths [14]. The use of NPs also roughens the surface, thereby increasing the active surface area and the scattering of light. As proposed by Paci et al., metallic nanoparticles have a dual advantage on the efficiency of OSCs. Along with the increase of path length of the absorbed light, nanoparticles also enhances the structural stability of the layer leading to a slower device degradation rate during prolonged illumination [5].

In this study, the artificial buffer layer mixed with metal oxide NPs (WO₃, MoO₃) was used to enhance the scattering effect and to provide a mechanical endurance to the device without increasing the thickness. For metallic NPs, Shockley–Read–Hall (SRH) recombination at interfacial traps [15] is proposed as the dominant mechanism at monomolecular and bimolecular recombination. Moreover, the electrochemical impedance spectroscopy (EIS) was used to study the interface charge transport process, resistance and constant phase element. The electrical and optical properties of the devices were analyzed.

2. Experiment details

We investigated the effect of metal oxide nanoparticle mixed in PEDOT:PSS-based buffer layer on the inverted organic solar cells. The size of both the particle used in this work was 100 nm. Poly (3-hexylthiophene):[6,6]-phenyl-C₆₁-butyric acid methyl ester (P3HT:PCBM) was used as an active layer. As shown in Fig. 1 (a), the fabricated

* Corresponding author at: School of Electronic and Electrical Engineering, Sungkyunkwan University, Suwon, Gyeonggi 440-746, Republic of Korea. Tel.: +82 31 299 4323.

E-mail address: yongsang@skku.edu (Y.-S. Kim).

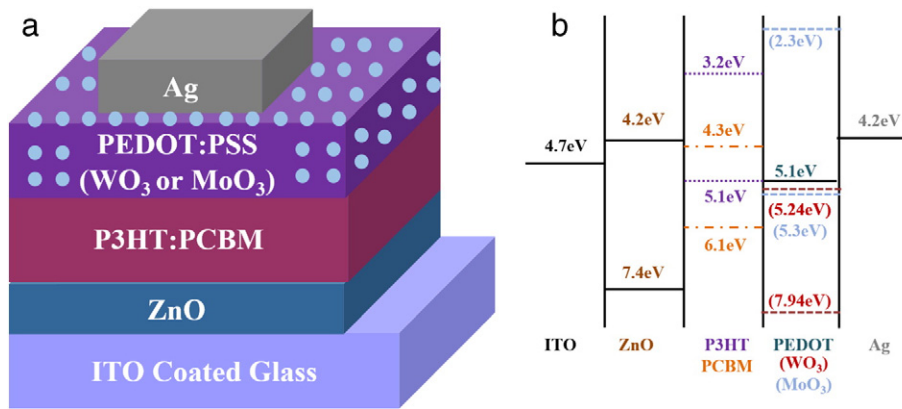


Fig. 1. (a) Schematic of the inverted organic solar cell showing ITO/ZnO/P3HT:PCBM/PEDOT:PSS(WO₃ or MoO₃)/Ag layers. (b) The energy band diagram with WO₃ and MoO₃ in PEDOT:PSS layer.

solar cells had a structure of ITO/ZnO/P3HT:PCBM/PEDOT:PSS (WO₃ or MoO₃)/Ag. For the fabrication, ITO glass substrates were cleaned in an ultrasonic bath with acetone, isopropyl alcohol, and deionized water for 20 min, respectively. ZnO was used as a buffer layer for hole blocking between the active layer and bottom electrode. At first, ZnO solution was spin coated on ITO substrate and then annealed at 200 °C for 20 min in a dry oven in ambient air. The active layer (P3HT:PCBM) was deposited on a ZnO layer by spin coating. The P3HT:PCBM mixture (P3HT:PCBM = 1:1 weight ratio) was dissolved in chlorobenzene at a concentration of 40 mg/ml. The thickness of the active layer was 200 nm in all the devices. In order to deposit hydrophilic PEDOT:PSS mixed with or without NPs on hydrophobic active layer, PEDOT:PSS was also mixed with 0.5 vol% of Triton X-100 (C₁₄H₂₂O(C₂H₄O)_n) non-ionic surfactant. This solution was then spin coated on hexamethylene disilazane, which was pre-coated on the active layer. Thermal pre-annealing was conducted at 160 °C for 10 min in a dry oven in ambient air. Ag top electrode (100 nm) was deposited on PEDOT:PSS layer through a shadow mask by thermal evaporation, defining an active area of 0.1 cm². The UV-visible spectrophotometer (Shimadzu UV-1601) was used to study light absorption of the active/buffer layers. Current density–voltage (*J*–*V*) characteristics were measured with *J*–*V* curve tracer (Eko MP-160) and a solar simulator (Yss-E40, Yamashita Denso) under AM 1.5G (100 mW/cm²) irradiation intensity. The impedance was measured using EIS. External quantum efficiency (EQE) spectra was measured under calibrated, monochromatic light illumination obtained from a xenon light source operating in the wavelength range of 300–700 nm (K3100, Mc Science). The light intensity was calibrated with a standard silicon cell (PV Measurements, Inc.). The output voltage of solar cells depends on the intensity of light. To study the light dependency, we altered the illumination intensity of solar simulator, by varying the power of the lamp power supply. The intensity of the illumination was checked every time before the measurement with a calibrated silicon cell and meter. Entire fabrication and measurement processes were conducted in ambient air.

3. Results and discussion

Fig. 1(a) and (b) shows the structure and energy band diagram of OSCs. The measured *J*–*V* characteristics of OSCs with PEDOT:PSS and PEDOT:PSS:WO₃ (different concentration) using a solar simulator is shown in Fig. 2(a). The control device showed a *J*_{sc} of 12.80 mA/cm². The addition of 0.1 wt% tungsten trioxide elevated the *J*_{sc} to 13.69 mA/cm². Increasing concentration of WO₃ NPs resulted in higher *J*_{sc}, but a threshold was seen at 1.5 wt%. At this concentration, the device gave a *J*_{sc} of 14.61 mA/cm² while the device with 5 wt% showed a lower *J*_{sc} of 13.22 mA/cm². The performance of devices improved due to light scattering. The performance of all the organic solar cells is summarized in Table 1. Use of 1.5 wt% WO₃ NPs increased the

*J*_{sc} by 14%. Fig. 1(b) shows the energy band diagram of our device. Many studies have shown the energy level of lowest unoccupied molecular orbital (LUMO) and highest occupied molecular orbital (HOMO) for WO₃ NPs at 5.24 eV and 7.94 eV, respectively. The higher concentration of WO₃ NPs increased the exciton generation. However, a very high concentration of the NPs interfered with the binding of PEDOT and PSS domains which reduced the carrier mobility. A blockage in holes migration reduced the current density directing to a lower PCE. The

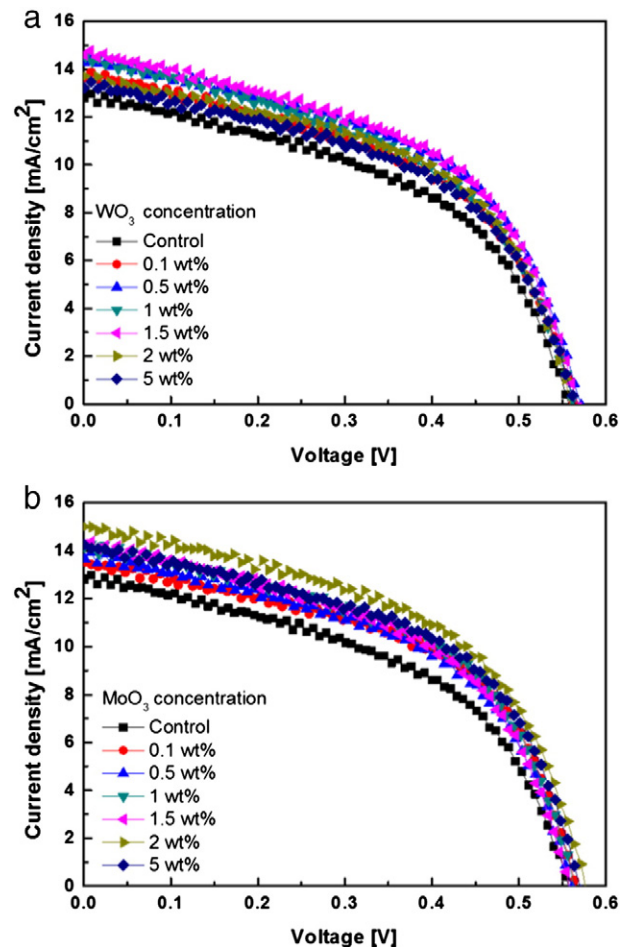


Fig. 2. (a) *J*–*V* characteristics of inverted organic solar cells using PEDOT:PSS buffer layer with different concentration of WO₃ NPs; (b) *J*–*V* characteristics of inverted organic solar cells using PEDOT:PSS buffer layer with different concentration of MoO₃ NPs; Under AM 1.5G irradiation at 100 mW/cm².

Table 1

Summary of organic solar cells performance with different concentrations of WO₃ NPs in PEDOT:PSS buffer layer.

WO ₃	<i>J</i> _{sc} [mA/cm ²]	<i>V</i> _{oc} [V]	Fill factor	PCE [%]
Control	12.80	0.56	0.48	3.46
0.1 wt%	13.69	0.56	0.49	3.84
0.5 wt%	14.31	0.57	0.50	4.03
1 wt%	14.53	0.56	0.50	4.06
1.5 wt%	14.61	0.56	0.51	4.22
2 wt%	13.69	0.56	0.51	3.93
5 wt%	13.22	0.56	0.51	3.79

NPs above 1.5 wt% concentration acts as an artificial hole blocking layer. The energy level of bulk layer is extensively reported, but the energy level of only NPs is seldom reported, which limits the study of the actual reason for the hole blockage layer formation at high nanoparticle concentration. A change in the energy level of WO₃ NP-based device prevents the transport of holes from P3HT:PCBM to silver electrode.

For comparison, we also used MoO₃ (100 nm) in place of WO₃ NPs in the buffer layer. The energy level of MoO₃ NPs at LUMO is 2.3 eV and at HOMO is 5.3 eV. All the devices were fabricated with the similar conditions. The concentration of MoO₃ in PEDOT:PSS ranged from 0.1% to 5%. The *J*-*V* curve of MoO₃ blended devices is shown in Fig. 2(b), while *J*_{sc} and PCE are plotted in the inset. The control device showed a *J*_{sc} of 12.80 mA/cm², whereas the device with an optimized concentration of 2 wt% MoO₃ NPs showed a *J*_{sc} of 15.00 mA/cm². The performance of all the organic solar cells is summarized in Table 2. The addition of MoO₃ NPs improved the hole transfer, a mechanism opposite to that of WO₃ NPs. A number of works have reported the use of metal oxide as buffer layer. A direct comparison of obtained results with previous literature is not possible, as most of the WO₃ and MoO₃ thin films were deposited using thermal evaporation. Recently, Zillberberg et al. [6] reported a PCE of 3.3% using thermally deposited MoO₃ thin film, and Tao et al. [8] reported a PCE of 2.58% using thermally deposited WO₃ thin film. However, in our work, we obtained a PCE of 4.4%. There were only a few attempts to use metallic NPs in organic solar cells. In a related work, Stubhan et al. used solution-processed MoO₃ thin film in a conventional structure but reported a very low light absorption and PCE of 2.92%. Similarly, Huang et al. [10] and Oh et al. [9] used solution-processed WO₃ NPs and reported a PCE of only 3.74% and 2.61%, respectively.

Fig. 3(a) shows the *J*-*V* characteristics of the best performing devices and control device. The black line (solid square) represents the control device, which showed a power conversion efficiency of 3.46%. The WO₃ and MoO₃-based devices showed the PCE of 4.22% and 4.40%, respectively. Fig. 3(b) shows the overall UV-visible absorption spectra. The black line represents the control device; in comparison, device with WO₃ NPs (1.5 wt%) or MoO₃ (2 wt%) shows more absorbance. The reason for this observation can be attributed to a phenomenon of formation of localized surface plasmon resonance (LSPR) and increase in scattering of light due to the use of metallic NPs, enhancing the light absorption efficiency. Fig. 3(c) shows the measured external quantum efficiency (EQE) of OSCs. A 25% increase in EQE was obtained due to the addition of MoO₃ NPs in PEDOT:PSS device. The EQE data

Table 2

Summary of organic solar cells performance with different concentrations of MoO₃ NPs in PEDOT:PSS buffer layer.

MoO ₃	<i>J</i> _{sc} [mA/cm ²]	<i>V</i> _{oc} [V]	Fill factor	PCE [%]
Control	12.80	0.56	0.48	3.46
0.1 wt%	13.52	0.56	0.51	3.96
0.5 wt%	13.71	0.56	0.51	3.99
1 wt%	14.18	0.56	0.51	4.07
1.5 wt%	14.29	0.56	0.51	4.12
2 wt%	15.00	0.57	0.51	4.40
5 wt%	14.26	0.57	0.51	4.17

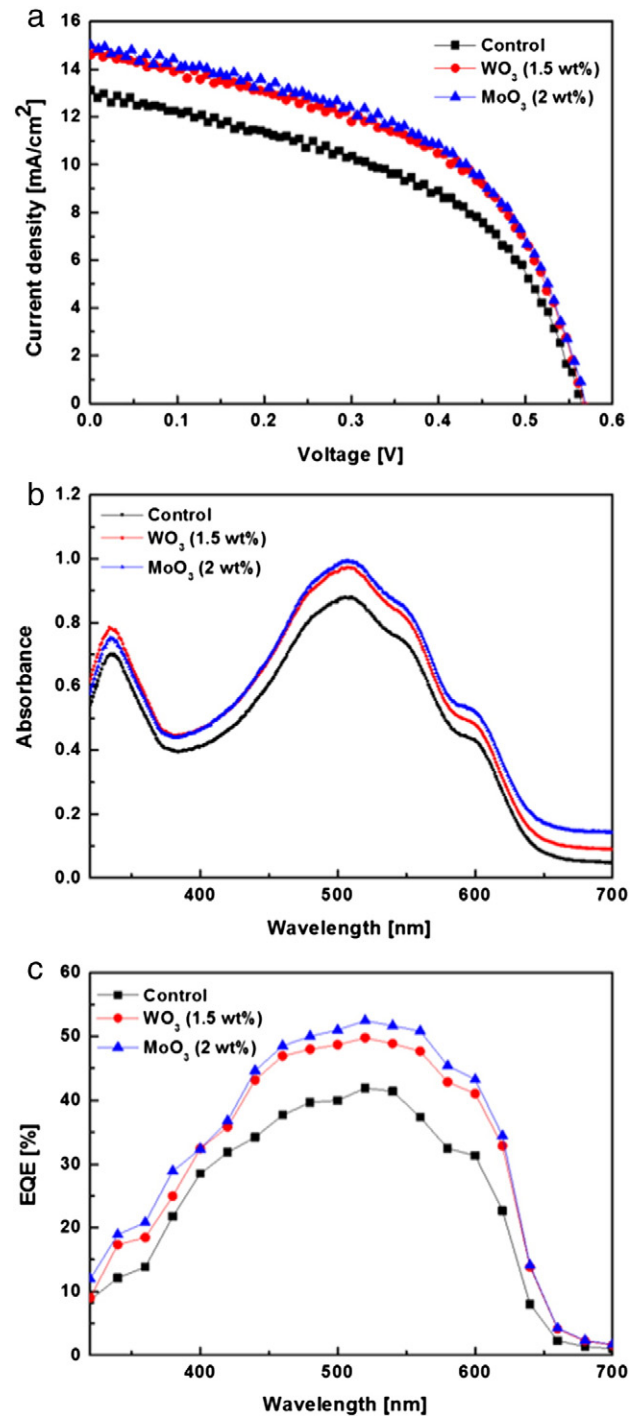


Fig. 3. (a) *J*-*V* characteristics of inverted organic solar cells using PEDOT:PSS buffer layer with WO₃ or MoO₃ NPs. (b) UV-visible absorption spectra with WO₃ or MoO₃ NPs in PEDOT:PSS layers. (c) The measurement of external quantum efficiency with WO₃ or MoO₃ NPs in PEDOT:PSS layers. (■): control, (●): with WO₃, (▲): with MoO₃.

support the electrical analysis and UV-visible data corresponding to Figs. 2 and 3(b).

Fig. 4(a) shows the semi-log plot of dependence of open-circuit voltage (*V*_{oc}) on the light intensity. The recombination studies at *V*_{oc} can provide detailed information of various mechanisms. The relationship between light intensity and *V*_{oc} is given by [16].

$$\delta V_{oc} = \frac{kT}{e} \ln(I) + \text{const.} \quad (1)$$

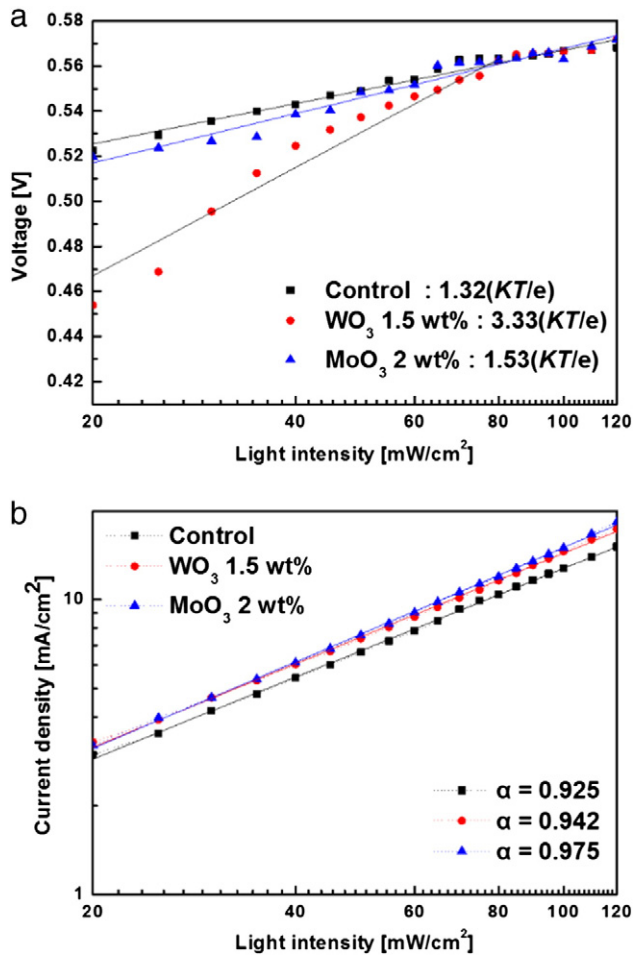


Fig. 4. (a) The measured V_{oc} of organic solar cells with WO_3 or MoO_3 NPs in PEDOT:PSS layers as a function of illumination intensity (symbols), together with linear fits of the data (solid lines). (b) Measured J_{sc} of organic solar cells with WO_3 or MoO_3 NPs in PEDOT:PSS layers plotted against light intensity (symbols) on the logarithmic scale and fitted yield α (dotted line). (—■—: control, —●—: with WO_3 , —▲—: with MoO_3).

where k is the Boltzmann constant, T is the temperature, e is the electronic charge, and I is the incident light intensity. When the additional mechanism of SRH trap-assisted recombination is involved, a stronger dependence of V_{oc} on light intensity with a slope greater than kT/e is observed. The control device showing a slope of $1.32(kT/e)$ is indicative of trap-assisted recombination. The addition of WO_3 and MoO_3 NPs in PEDOT:PSS layer gave a slope value of $3.33(kT/e)$ and $1.53(kT/e)$, respectively, confirming the trap-assisted recombination. The slope value of WO_3 -based devices increased because the low intensity mode of WO_3 device prevents the hole transfer, which increases monomolecular recombination.

The J_{sc} can be correlated to light intensity (I) by [16].

$$J_{sc} \propto I^\alpha (\alpha \leq 1). \quad (2)$$

At short circuit, the bimolecular recombination should be minimum ($\alpha \approx 1$) [17]. Fig. 4(b) shows the log–log scale relationship of J_{sc} as a function of light intensity. The fitting of the data yielded $\alpha = 0.925$ for control device, which can be attributed to the bimolecular recombination. The device with WO_3 and MoO_3 NPs in PEDOT:PSS layer gave an α value of 0.942 and 0.975, respectively. The J_{sc} vs. I data prove the J – V characteristics shown in Fig. 3(a) because the bimolecular recombination is close to minimum at J_{sc} .

Fig. 5(a) and (b) shows the frequency-dependent real and imaginary parts of the impedance of the devices with NPs in PEDOT:PSS. Fig. 5(a) indicates that the real part of impedance is attributed by two

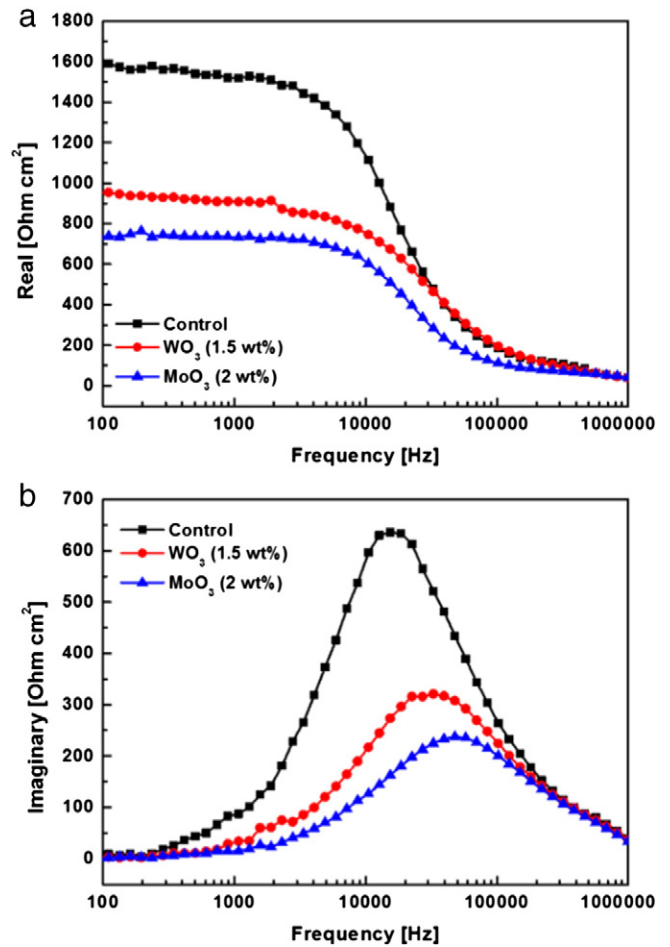


Fig. 5. (a) The frequency-dependent real parts; (b) the frequency-dependent imaginary parts in the impedance spectra of the devices with WO_3 or MoO_3 NPs in PEDOT:PSS layers (—■—: control, —●—: with WO_3 , —▲—: with MoO_3).

types of resistance, which is low frequency (<100 Hz) and high frequency (>5000 Hz), respectively. The low-frequency region of impedance corresponds to the parasitic resistance (R_p), and the high-frequency region is attributed to the series resistance (R_s) [17,18]. The constant phase element (CPE) is often used in place of a capacitance-like element to compensate for non-homogeneity in the interface. CPE is defined by two values, CPE-T and CPE-P. The CPE-T may be distributed along the surface of an electrode or in the direction normal to the electrode. Distributions of CPE-T result from distributions of physical properties, including structure, reactivity, and resistivity. If CPE-P equals 1, then the CPE is identical to an ideal capacitor without defects and/or grain boundary [18]. The control device showing an R_p of $1602 \Omega \cdot \text{cm}^2$. The addition of WO_3 and MoO_3 NPs in PEDOT:PSS layer gave a parasitic resistance of $965 \Omega \cdot \text{cm}^2$ and $664 \Omega \cdot \text{cm}^2$, respectively. The values of R_p is the smallest for the device with MoO_3 NPs in PEDOT:PSS layer. This indicates that the charge transport between P3HT and PCBM of MoO_3 NP-based cell is the best. The value of R_p is highly sensitive to the morphology of a charge transport layer. The performance of all the organic solar cells is summarized in Table 3. Fig. 5(b) shows the

Table 3

EIS measurement of organic solar cells without NPs, with WO_3 (1.5 wt%) and MoO_3 (2 wt%) NPs in PEDOT:PSS layer.

	R_s [$\Omega \text{ cm}^2$]	R_p [$\Omega \text{ cm}^2$]	CPE-T [$\mu\text{F}/\text{cm}^2$]	CPE-P
Control	39	1602	0.63	0.97
WO_3	38	965	0.51	0.97
MoO_3	35	664	0.39	0.98

frequency-dependent imaginary part of impedance of the different devices. This plot is usually used to evaluate the relaxation frequency of most resistive contribution. The frequency (f_{\max}) centered at peak position represents the carrier transfer rate. The control device showed a f_{\max} of 15360 Hz. The addition of WO_3 and MoO_3 NPs in PEDOT:PSS layer gave a maximum frequency of 32820 Hz and 47970 Hz, respectively. The value of f_{\max} of the device with MoO_3 NP in PEDOT:PSS layer is largest among all devices. Thus, τ value of the device with MoO_3 NPs is smallest of all the devices. The values can be defined by the relation: $f_{\max} \propto 1/\tau$. The small τ suggests efficient dissociation of exciton at the interface between P3HT and PCBM and charge transport in the active layer. Also, the proceeding time of electrons at the interface is short, which suggests efficient charge transport on the interface between the active layer and electrode. As a result, the small τ could lead to the enhancement of J_{sc} .

4. Conclusion

The effects of two kinds of metal oxide NPs in PEDOT:PSS layer for light harvesting on organic solar cells was investigated. The addition of metallic NPs increased the light scattering. The control device showed a 3.46% efficiency while WO_3 NPs in PEDOT:PSS layer showed a PCE of 4.22%. The device with MoO_3 NPs in PEDOT:PSS layer showed a higher performance of 4.40% under AM 1.5G illumination. Upon investigation, it was seen that the tungsten trioxide nanoparticles acted as a hole blocking layer, whereas molybdenum trioxide nanoparticles helped in hole transfer. The difference in the energy band of two NPs with that of PEDOT:PSS resulted in the contrasting effect. WO_3 NP-based device showed a monomolecular recombination of 3.33 (kT/e), while MoO_3 NPs in PEDOT:PSS layer gave a value of 1.53 (kT/e), which confirms the trap-assisted recombination. The MoO_3 NP-based devices have low parasitic resistance and bimolecular, monomolecular recombination property.

Acknowledgments

This work was supported under the framework of international cooperation program managed by National Research Foundation of Korea (no. 2014K2A2A2000803) and also supported by the Human Resources Development program (no. 20124010203280) of the Korea Institute of Energy Technology Evaluation and Planning (KETEP) grant funded by the Korea government Ministry of Trade, Industry and Energy.

References

- [1] H.Y. Chen, J.H. Hou, S.Q. Zhang, Y.Y. Liang, G.W. Yang, Y. Yang, L.P. Yu, Y. Wu, G. Li, Polymer solar cells with enhanced open-circuit voltage and efficiency, *Nat. Photonics* 3 (2009) 649.
- [2] J.H. Hou, H.Y. Chen, S.Q. Zhang, R.I. Chen, Y. Yang, Y. Wu, G. Li, Synthesis of a low band gap polymer and its application in highly efficient polymer solar cells, *J. Am. Chem. Soc.* 131 (2009) 15586.
- [3] Y.Y. Liang, Z. Xu, J.B. Xia, S.T. Tsai, Y. Wu, G. Li, C. Ray, L.P. Yu, For the bright future-bulk heterojunction polymer solar cells with power conversion efficiency of 7.4%, *Adv. Mater.* 22 (2010) E135.
- [4] K.M. Coakley, M.D. McGehee, Conjugated polymer photovoltaic cells, *Chem. Mater.* 16 (2004) 4533.
- [5] B. Paci, G.D. Spyropoulos, A. Generosi, D. Bailo, V.R. Alberini, E. Startakis, E. Kymakis, Enhanced structural stability and performance durability of bulk heterojunction photovoltaic devices incorporating metallic nanoparticles, *Adv. Funct. Mater.* 21 (2011) 3573.
- [6] K. Zillberberg, H. Gharbi, A. Behrendt, Sara Trost, T. Riedl, , Low-temperature, solution-processed MoO_x for efficient and stable organic solar cells, *Appl. Mater. Interfaces* 4 (2012) 1164.
- [7] D.W. Zhao, P. Liu, X.W. Sun, S.T. Tan, L. Ke, A.K.K. Kyaw, An inverted organic solar cells with an ultrathin Ca electron-transporting layer and MoO_3 hole-transporting layer, *Appl. Phys. Lett.* 95 (2009) 153304.
- [8] C. Tao, S. Ruan, G. Xie, X. Kong, L. Shen, F. Meng, C. Liu, X. Zhang, W. Dong, W. Chen, Role of tungsten oxide in inverted polymer solar cells, *Appl. Phys. Lett.* 94 (2009) 043311.
- [9] I.S. Oh, G.M. Kim, S.H. Han, S.Y. Oh, PEDOT:PSS-Free organic photovoltaic cells using tungsten oxides as buffer layer on anodes, *Electron. Mater. Lett.* 9 (2013) 375.
- [10] J.S. Huang, C.Y. Chou, C.F. Liu, Efficient and air-stable polymer photovoltaic devices with WO_3 - V_2O_5 mixed oxides as anodic modification, *IEEE Electron. Device Lett.* 31 (2010) 332.
- [11] T. Stubhan, T. Ameri, M. Salinas, J. Krantz, F. Machui, M. Halik, C.J. Brabec, High shunt resistance in polymer solar cells comprising a MoO_3 hole extraction layer processed from nanoparticle suspension, *Appl. Phys. Lett.* 98 (2011) 253308.
- [12] K.R. Choudhury, J.W. Lee, N. Chopra, A. Gupta, X.Z. Jiang, F. Amy, F. So, Highly efficient hole injection using polymeric anode materials for small-molecule organic light-emitting diodes, *Adv. Funct. Mater.* 19 (2009) 491.
- [13] T.W. Lee, M.G. Kim, S.Y. Kim, S.H. Park, O. Kwon, T. Noh, T.S. Oh, Hole-transporting interlayers for improving the device lifetime in the polymer light-emitting diodes, *Appl. Phys. Lett.* 89 (2006) 123505.
- [14] W.L. Barnes, A. Dereux, T.W. Ebbesen, Surface plasmon subwavelength optics, *Nature* 424 (2003) 824.
- [15] I. Yoo, M. Lee, C. Lee, D.W. Kim, I.S. Moon, D.H. Hwang, The effects of a buffer layer on the photovoltaic properties of solar cells with P3OT:fullerene composites, *Synth. Met.* 153 (2005) 97.
- [16] S.R. Cowan, A. Roy, A.J. Heeger, Recombination in polymer-fullerene bulk-heterojunction solar cells, *Phys. Rev. B* 82 (2010) 245207.
- [17] Y. Zhang, L. Li, S. Yuan, G. Li, W. Zhang, Electrical properties of the interfaces in bulk heterojunction organic solar cells investigated by electrochemical impedance spectroscopy, *Electrochim. Acta* 109 (2013) 221.
- [18] G. Perrier, R.D. Bettignies, S. Berson, N. Lemaitre, S. Guillerez, Impedance spectroscopy of optimized standard and inverted P3HT:PCBM organic solar cells, *Sol. Energy Mater. Sol. Cells* 101 (2012) 210.